Kochi Chapter

Indian Geotechnical Conference
IGC 2022
15th – 17th December, 2022, Kochi

# Sensitivity of Trapped Stiff Layer in the Field Acquisition of Rayleigh Wave using MASW

Mrinal Bhaumik [1][0000-0001-8906-0971] and Tarun Naskar [2][0000-0002-2752-2840]

[1] Indian Institute of Technology Madras, Chennai, India
[2] Indian Institute of Technology Madras, Chennai, India

[1]ce19d757@smail.iitm.ac.in
[2]tarunnaskar@civil.iitm.ac.in

**Abstract.** Vertical component acquisition of Rayleigh wave is the most widely used technique for Multichannel Analysis of Surface Wave (MASW). Dispersion imaging of the acquired field data is a critical step in determining the in-situ shear wave velocity profile by performing in- version analysis. The presence of trapped stiff or soft layers is common in real-world situations, and identifying such irregularities from disper- sion images is crucial for an accurate inversion analysis. It is well known that the presence of a soft or low-velocity layer breaks the continuity of the fundamental mode and influences the higher modes, i.e., higher modes will carry more energy. However, the presence of a trapped stiff layer doesn't affect modes significantly in the dispersion image. In the present study, we have investigated the role of trapped stiff layers in the dispersion energy of the Rayleigh wave. The sensitivity of the trapped layers has been quantified by analyzing the Jacobian matrix. Further, the dispersion image of the corresponding synthetic earth profile is generated from the seismogram obtained by the standard staggered grid finite-dif- ference modeling. This study shows that it is difficult to capture the pres- ence of a trapped stiff layer using only the vertical component MASW method.

**Keywords:** MASW; Sensitivity; Shear wave velocity; Rayleigh wave; Jacobian

## 1 Introduction

The multichannel analysis of surface wave (MASW) is widely adopted to obtain shear wave velocities of a few top ten meters of the sub-surface. The MASW method is performed by acquiring Rayleigh wave with different components (vertical or transverse) or Love wave[1–3]. However, the vertical component-based MASW is commonly practiced among geotechnical engineers. The standard procedure of surface wave analysis is performed in three main stages: (i) acquisition of multichannel data, (ii) processing of time domain data to develop field dispersion image, and (iii) inversion of field dispersion curves to estimate shear wave velocity profile. The quality of the dispersion image greatly influences the accuracy of the inverse analysis, especially when higher modes are present. In practice, layered profiles are usually assumed to be regularly

dispersive, however this is not always true. Because of the complex irregularities in the layered model, the spectral energy distribution in the dispersion image is complicated in the real world. The presence of a low-velocity layer (LVL) and a high-velocity layer (HVL) or stiff layer are two typical irregularities observed in the layered geological model. An LVL refers to a layer whose shear wave velocity is lower than at least a layer above it [4]. The low velocity may occur due to the presence of saturated soft clay or loose sand type layers, which is widely observed in the near-surface earth profiles. Similarly, HVL is a stiff layer with a shear wave velocity higher than the layers above and below it [5]. The presence of a shallow stiff layer is common in the urbanized area.

The sensitivity of each layer plays a crucial role in inverse analysis. A layer with low sensitivity is poorly reconstructed through inversion[6–8]. An MASW survey on an LVL type profile develops a discontinuous dispersion image. The soft layer stimulates the jumping of modal energy from fundamental mode to higher mode and may not return to the fundamental mode[1, 9, 10]. The LVL layers are easily susceptible, and their presence is immediately observed in the dispersion image [4]. Thus, an appropriate inversion scheme can easily reconstruct an LVL model if the higher modes are considered. On the other hand, the presence of HVL doesn't always excite the higher mode[5, 11]. Dal Moro [5] studied the influence of a thin HVL placed at the surface and found no change in the dispersion spectrum due to the stiff surface layer. However, the appearance of HVL on dispersion image depends upon several other factors, such as depth of embedment, thickness, and velocity contrast of the stiff layer. Shen et al [11] found that the HVL is poorly sensitive to the theoretical fundamental mode. Nevertheless, layer irregularities may excite the higher modes; therefore, it is necessary to study the dominant mode or the entire dispersion spectrum.

This paper investigates the sensitivity of stiff layers on surface wave dispersion where the stiff layer with different velocity contrast is positioned at various depths. The sensitivity of the soil profile is studied by analyzing the Jacobian matrix, which is a partial derivative of Rayleigh wave phase velocity with respect to medium parameters. A numerical analysis is performed to observe the distribution of dispersion energy at a different frequency. The study shows that the overall sensitivity of the medium reduces due to the presence of a stiff layer. The sensitivity of the high velocity stiff layer drastically decreases with the velocity contrast and depth of embedment.

## 2 Computation of Sensitivity

For a layered earth model, the wave equation, after applying proper boundary condition and free surface condition, turns into a characteristic equation in its nonlinear, implicit form [6]:

$$F(f_i, V_{Ri}, v_s, v_p, \rho, h) = 0 \qquad (i = 1, 2, 3, \ldots, m) \qquad (1)$$

where $f_i$ is the frequency in Hz; $V_{Rj}$ is Rayleigh wave phase velocity corresponding to the frequency $f_i$; $v_p = (v_{p1}, v_{p2}, \ldots, v_{pn})^T$ is the compressional wave velocity vector; ; $v_s = (v_{s1}, v_{s2}, \ldots, v_{sn})^T$ is the shear wave velocity vector; $\rho = (\rho_1, \rho_2, \ldots, \rho_n)^T$ is the density vector; $n$ is the number of layers and $h = (h_1, h_2, \ldots, h_{n-1})^T$. Therefore, the four basic parameters can physically define a homogeneous, isotropic, horizontally

layered media. Each parameter is uniquely sensitive to the Rayleigh wave's velocity at specific frequencies. However, $v_p$ and $\rho$ are relatively less sensitive to phase velocity compared to $v_s$. Thus only $v_s$ is studied by keeping the Poisson's ratio and $\rho$ constant or known.

For a generalized linear inversion process, such as Levenberg-Marquardt (L-M) algorithm, the sensitivity kernel is essential to determine the adjustment of parameters towards convergence of inversion. Thus, equation 1 can be linearized by Taylor series expansion [6]:

$$\mathbf{J}_{v_s}\Delta\mathbf{v_s} = \Delta\mathbf{b} \tag{2}$$

where, $\mathbf{b}$ is the Rayleigh wave phase velocity vector, $\mathbf{b} = [b_1, b_2, \dots, b_m]^T$.$\Delta\mathbf{b}$ is the difference between the observed phase velocity from the dispersion image and the estimated phase velocity of the initial model $v_{s0}$.

$$\Delta\mathbf{b} = [(b_R^{obs} - V_R(v_{s0}))_{f=f1}, (b_R^{obs} - V_R(v_{s0}))_{f=f2}, \dots, (b_R^{obs} - V_R(v_{s0}))_{f=fm}]^T \tag{3}$$

$\Delta\mathbf{v_s}$ is the adjustment vector of the initial model $v_{s0}$ of length $n$. $\mathbf{J}_{v_s}$ is the Jacobian matrix or sensitivity kernel (thin and tall matrix) with $m$ rows and $n$ columns ($m > n$).

The elements of the Jacobian matrix are the first-order partial derivative of phase velocities ($V_R$) with respect to shear wave velocities.

$$\mathbf{J}_{v_s} = \begin{bmatrix} \left(\frac{\partial V_r}{\partial v_{s1}}\right)_{f=f_1} & \left(\frac{\partial V_r}{\partial v_{s2}}\right)_{f=f_1} & \cdots & \left(\frac{\partial V_r}{\partial v_{sn}}\right)_{f=f1} \\ \left(\frac{\partial V_r}{\partial v_{s1}}\right)_{f=f_2} & \left(\frac{\partial V_r}{\partial v_{s2}}\right)_{f=f_2} & \cdots & \left(\frac{\partial V_r}{\partial v_{sn}}\right)_{f=f2} \\ \vdots & \vdots & \ddots & \vdots \\ \left(\frac{\partial V_r}{\partial v_{s1}}\right)_{f=f_m} & \left(\frac{\partial V_r}{\partial v_{s2}}\right)_{f=f_m} & \cdots & \left(\frac{\partial V_r}{\partial v_{sn}}\right)_{f=fm} \end{bmatrix}_{m\times n} \tag{4}$$

The partial derivatives can be calculated numerically using Ridder's method of polynomial extrapolation.

The sensitivity kernel, $\mathbf{J}_{v_s}$not only decide the parameters updation in inverse analysis, but also describe the contribution of any layer on the surface wave dispersion. Low sensitive layers have less involvement in wave propagation thus they are less susceptible to be detected through inverse analysis, which also enhances the non-uniqueness of inversion analysis.

## 3 Numerical Modelling of Surface Wave

It should be mentioned that the sensitivity value of any layer is different for each mode. Based on the corresponding soil profile's dispersion image, it is possible to determine whether higher modes should be studied or not. Thus, along with the sensitivity kernel, this study analyses the dispersion energy of Rayleigh waves using staggered grid finite

difference wavefield modeling. Staggered grid methods are widely used for elastic wavefield modeling (velocity-stress formulation) because of their high computational efficiency and easy implementation [12]. A staggered grid has several advantages over an ordinary finite difference method and other numerical methods discussed by Moczo [13]. Unlike the conventional finite difference scheme, the displacement/velocity component and each stress component have their own location in the staggered grid formulation.

The first-order velocity-stress formulation of the wave equation can be written as:

$$\begin{gathered}\rho\frac{\partial v_x}{\partial t}=\frac{\partial \sigma_{xx}}{\partial x}+\frac{\partial \tau_{xz}}{\partial z}\\ \rho\frac{\partial v_z}{\partial t}=\frac{\partial \tau_{xz}}{\partial x}+\frac{\partial \sigma_{zz}}{\partial z}\\ \frac{\partial \sigma_{xx}}{\partial t}=(\lambda+2\mu)\frac{\partial v_x}{\partial x}+\lambda\frac{\partial v_z}{\partial z}\\ \frac{\partial \sigma_{zz}}{\partial t}=(\lambda+2\mu)\frac{\partial v_z}{\partial z}+\lambda\frac{\partial v_x}{\partial x}\\ \frac{\partial r_{xz}}{\partial t}=\mu\left(\frac{\partial v_x}{\partial z}+\frac{\partial v_z}{\partial x}\right)\end{gathered} \tag{5}$$

where,$\sigma_{xx}$ , $\sigma_{zz}$ are normal stresses, and $r_{xz}$ is shear stress; $v_x$, $v_z$ are the velocity component in $x$ and $z$ direction, respectively. The standard staggered grid discretization of the Equation 5 is illustrated in Fig1.

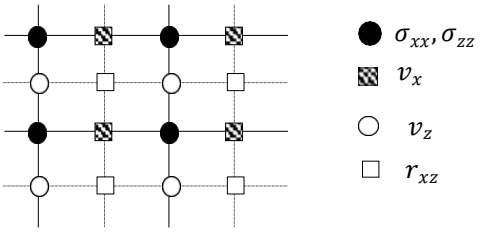


**Fig.1.** Finite difference staggered grid discretization

## 4 Sensitivity of Stiff Layers

A six-layer regularly dispersive earth model (Table 1) [6] is taken as a representative profile to investigate the stiff layers at different depths. A high velocity stiff layer with different velocity contrast is placed at the 2nd,3rd, and 4th layer's positions in the model (Fig 2) and the sensitivity of the different layers is studied using equation 4. Each layer's "total relative sensitivity" is calculated by summing up all the normalized sensitivity values at each frequency and dividing by the number of frequency samples. The total relative sensitivity of any layer describes the layer's overall contribution to the surface wave dispersion.

A 50 Hz Ricker wavelet is used to model the surface hammer blow in the numerical simulation. For every soil model, vertical component synthetic data is recorded at 48

receiver locations spaced every 1 m. The dispersion image is generated using the phase shift transform method [14–16].

**Table 1**. Six-layer subsurface model.

| Layer no | S-wave velocity (m/s) | Poisson's Ratio | Density ($kg/m^3$) | Thickness (m) |
|---|---|---|---|---|
| 1 | 194 | 0.430 | 1780 | 2 |
| 2 | 270 | 0.396 | 1820 | 2.3 |
| 3 | 367 | 0.447 | 1870 | 2.5 |
| 4 | 485 | 0.443 | 1920 | 2.8 |
| 5 | 603 | 0.439 | 1980 | 3.2 |
| 6 | 740 | 0.446 | 2050 | ∞ |

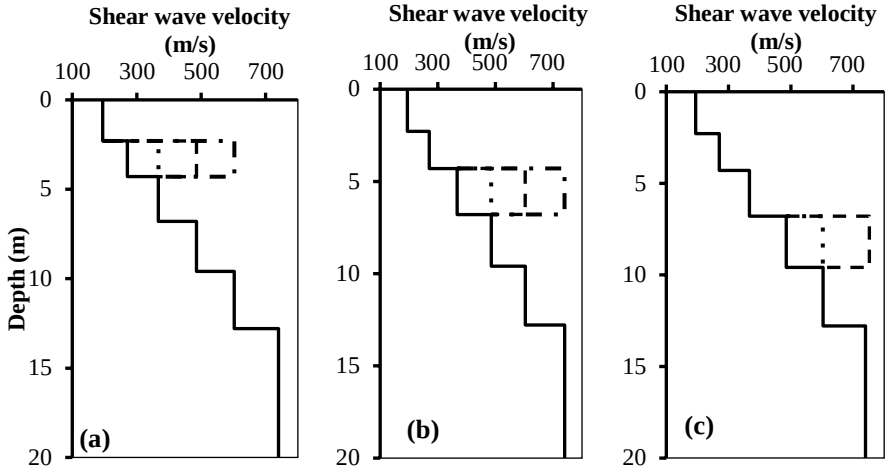


**Fig. 1**. Stiff layer at different depths, (a) HVL at 2nd layer, (b) HVL at 3rd layer, and (c) HVL at 4th layer.

### 4.1 HVL at the second layer

The sensitivity kernel of the original profile is shown in Fig 2a. It can be seen that, the high frequencies (> 40 Hz) are predominantly influenced by the top layer since the shorter wavelengths are confined near the surface, and the low frequencies (<15 Hz) are excited mainly by half-space. The middle layers are sensitive to the intermediate frequency range (15-40) depending upon their layer parameters. According to the overall sensitivity, the top layer is the most sensitive, and the 5th layer is the least sensitive. The corresponding dispersion image is presented in Fig 2b, where the white dotted lines are the theoretical modes obtained by the stiffness matrix method [17–19]. It can be observed that the fundamental mode dominates almost across all the frequencies. Fig 2c presents the sensitivity kernel when $v_s$ of the 2nd layer is increased by 1.36 times to make it the same as the $v_s$ of 3rd layer. It is clearly visible that the sensitivity of the 2nd layer drastically reduced, and the energy distribution of the dispersion image also changed (Fig 2d). However, the overall sensitivity of the layers is enough to be captured

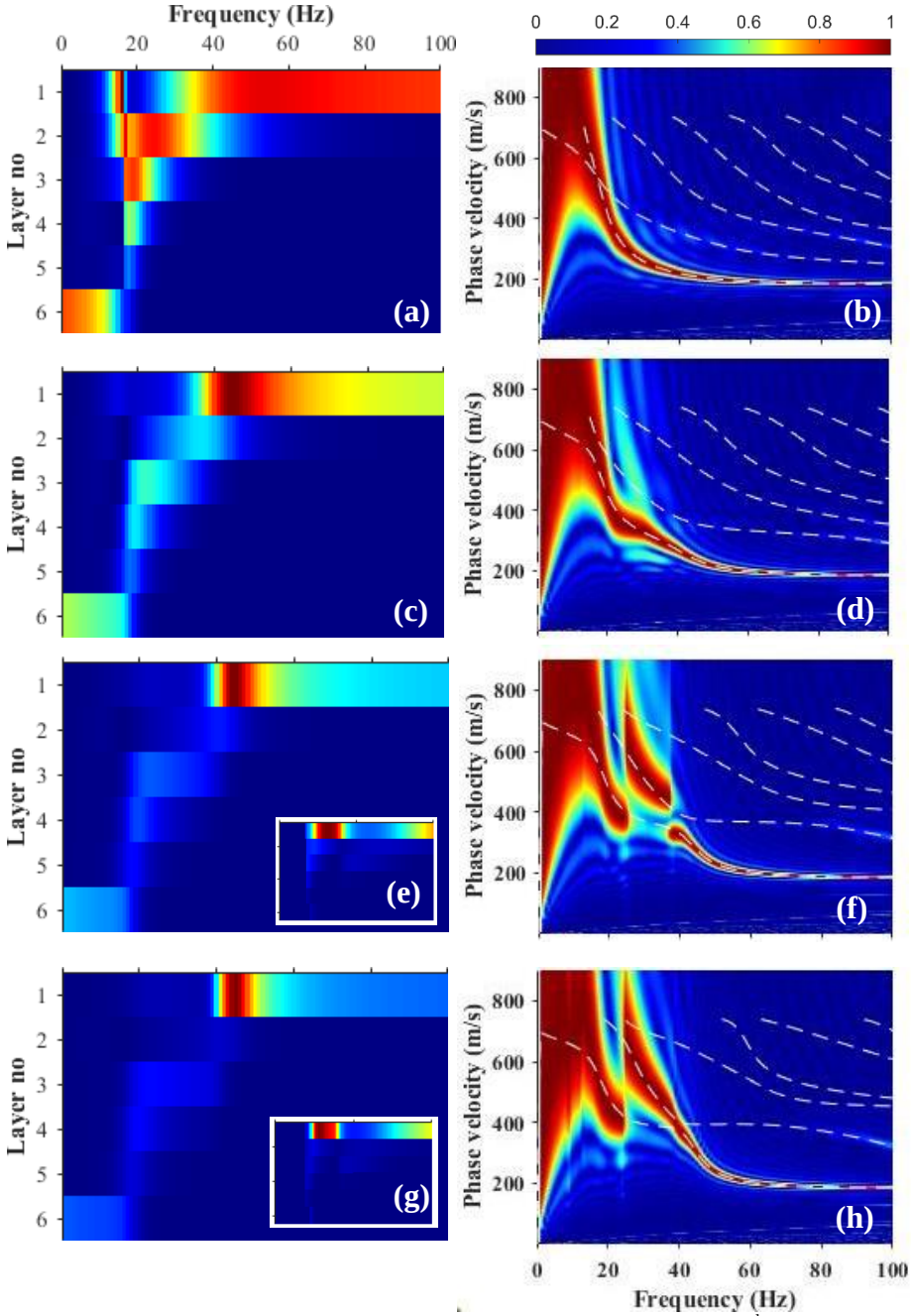


**Fig. 2.** Sensitivity kernel and dispersion image of HVL positioned at 2nd layer, (a) sensitivity of original profile, (b) dispersion image of original profile, (c) sensitivity of HVL of velocity ratio 1.36, (d) corresponding dispersion image, (e) sensitivity of HVL of velocity ratio 1.8, (f) corresponding dispersion image, (g) sensitivity of HVL of velocity ratio 2.23, and (h) corresponding dispersion image.

through inversion. Fig 2e illustrates the sensitivity kernel when the $v_s$ is increased by 1.8 times. It is observed that the overall relative sensitivity is further reduced. The corresponding dispersion image in Fig 2f shows a clear modal energy jumping from fundamental mode to 1st higher mode in a frequency range of 20 to 40 Hz. As the higher mode is also excited, the sensitivity of 1st higher mode is calculated. However, it can be seen from Fig 2e (right bottom corner) that the 1st layer is more sensitive even for higher mode. And more interestingly, the modal energy returns back to the fundamental mode, which doesn't happen in the presence of LVL. Similarly, in Fig 2g, the stiff layer velocity is increased by 2.23 times, which further reduces the sensitivity.

The variation of overall sensitivity for different shear wave velocity ratios of the stiff embedded layer is shown in Fig 3. The red line corresponds to the stiff layer.

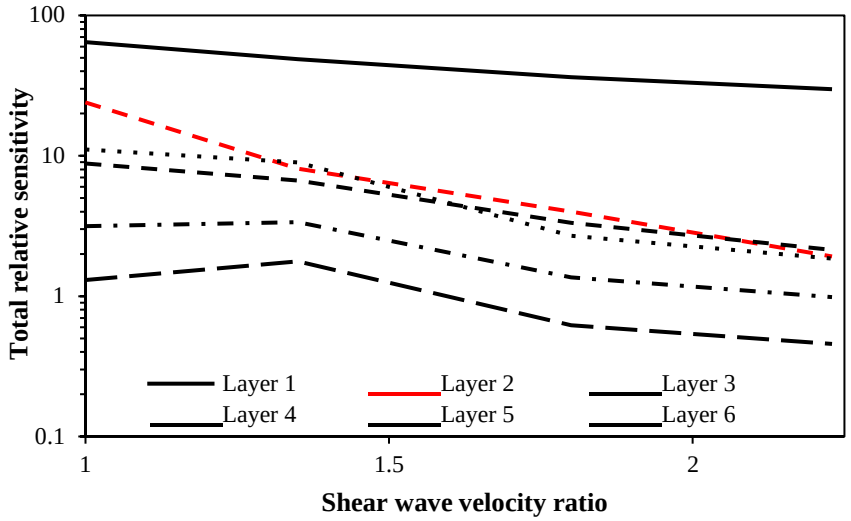


Fig. 3. Variation of total sensitivity at different shear wave velocity ratio of 2nd layer

### 4.2 HVL at the third layer

Let's consider the stiff layer is at 3rd layer of the model (Fig 1b). Fig 4a and 4b are the sensitivity kernel of the fundamental mode and dispersion images of the original profile, respectively. Fig 4c shows the sensitivity of the model when $v_s$ of the third layer is increased by 1.32 times. Similar to the results discussed in earlier example, the overall sensitivity of the layers other than the one immediately below the HVL is reduced. This model does not exactly represent an HVL model since $v_s$ of the third layer is identical to $v_s$ of the fourth layer. However, this is studied to observe the influence on sensitivity. The corresponding dispersion image is plotted in Fig 4d. Compare to the original dispersion image (Fig 4b), no significant change is observed in the spectral energy distribution. The $v_s$ of the third layer is then increased by 1.64 times to make it equal to next higher stiff layer. The overall sensitivity of the layers is further reduced (Fig 4e). However, the dispersion trends are almost similar to the original one. Studying the theoretical dispersion curves, a shift in modal osculation point towards high frequency is observed. The $v_s$ of the HVL is further increased to make it same to the next higher $v_s$, and the corresponding sensitivity kernel and dispersion image is plotted in Fig 4g

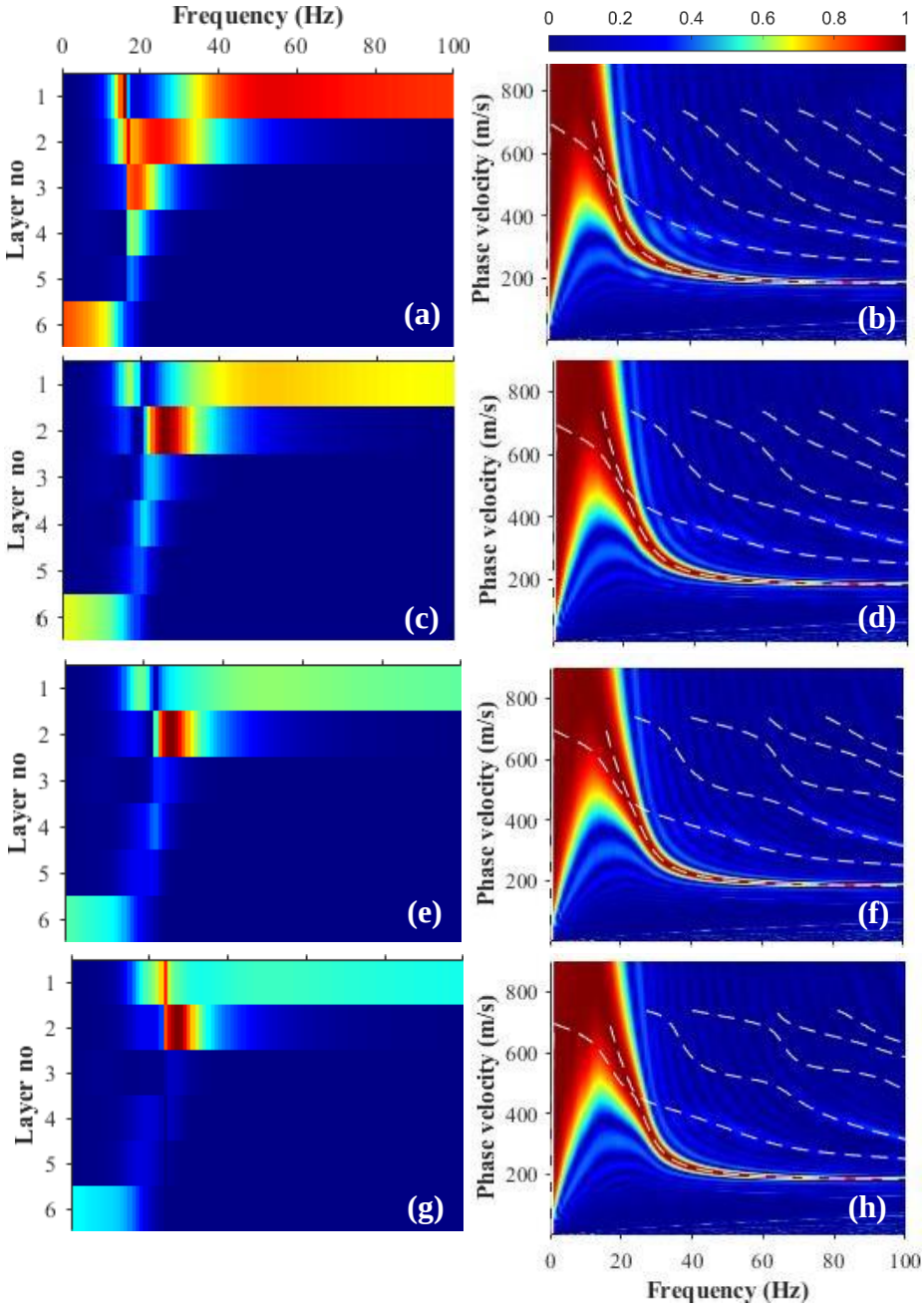


**Fig. 4** Sensitivity kernel and dispersion image of HVL positioned at 3rd layer, (a) sensitivity of original profile, (b) dispersion image of original profile, (c) sensitivity of HVL of velocity ratio 1.36, (d) corresponding dispersion image, (e) sensitivity of HVL of velocity ratio 1.8, (f) corresponding dispersion image, (g) sensitivity of HVL of velocity ratio 2.23, and (h) corresponding dispersion image.

and 4h, respectively. The overall change in sensitivity of individual layer with different $v_s$ ratio of the 3rd layer is illustrated in Fig 5. It is observed that the sensitivity of each layer decreases with an increase in the stiffness of the stiff layer. Especially, the sensitivity of HVL (red dotted line) reduces significantly compared to other layers.

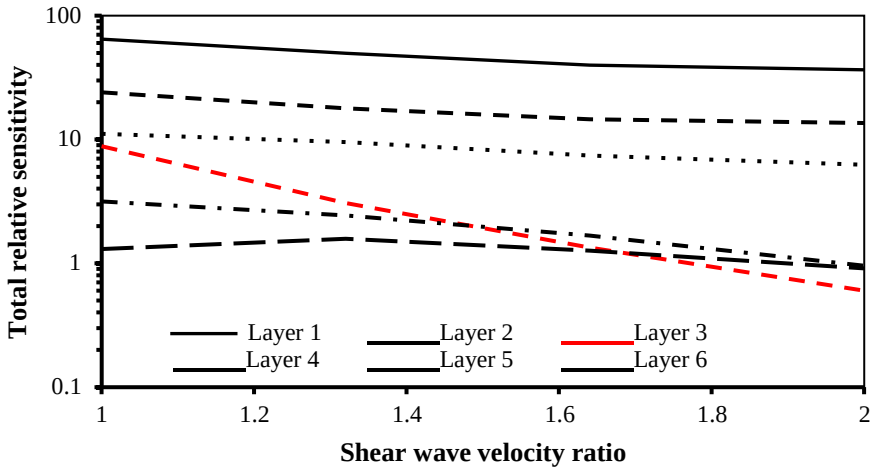


**Fig. 5**. Variation of total sensitivity at different shear wave velocity ratio of 3rd layer

### 4.3 HVL at the fourth layer

Now the HVL is placed at the 4th layer of the model (Fig 1c) and corresponding sensitivity kernel and dispersion image are plotted in Fig 6. The velocity of the 4th layer is increased to 603 m/s, which is same as the 5th layer. Comparing the sensitivity kernel (Fig 6c) with the original profile's sensitivity kernel (Fig 6a), it is clear that the overall sensitivity decreases. A similar trend is observed when the layer stiffness further increased by 1.52 times, to make the $v_s$ same as the next maximum layer. The dispersion image of the HVL profiles is almost same as the original profile, although the sensitivity of the stiff layer decreases. The comparison of overall sensitivity of each layer at different shear wave velocity ratio is presented in Fig 7. It can be observed that overall sensitivity decreases with the increment of velocity contrast of the stiff layer. Similar to the earlier cases, the decrement rate is higher for the stiff layer compare to other layers.

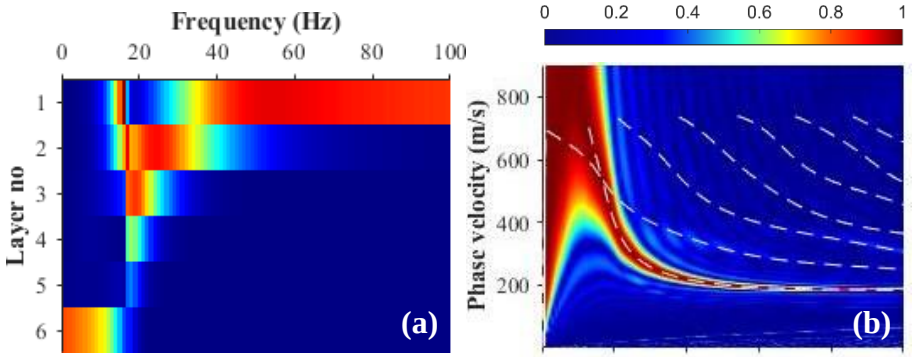

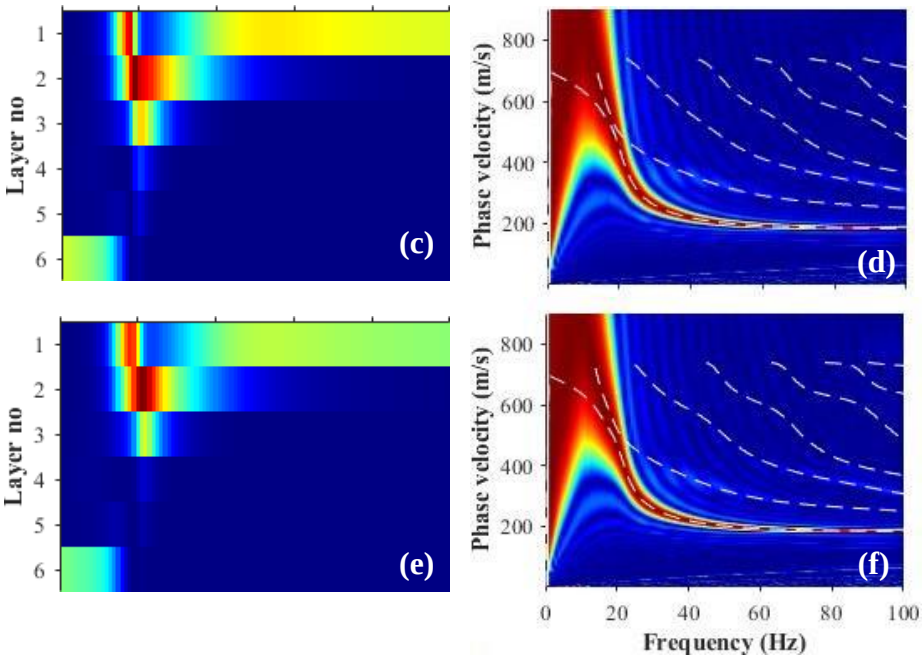


**Fig. 6.** Sensitivity kernel and dispersion image of HVL positioned at 4th layer, (a) sensitivity of original profile, (b) dispersion image of original profile, (c) sensitivity of HVL of velocity ratio 1.36, (d) corresponding dispersion image, (e) sensitivity of HVL

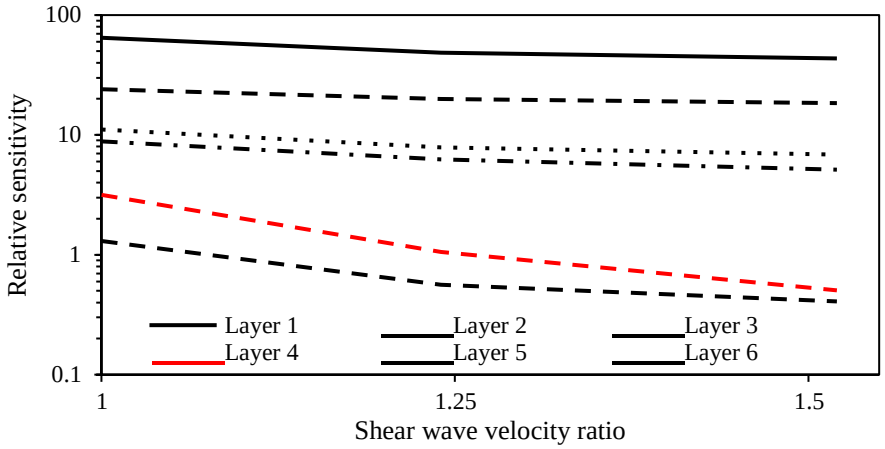


**Fig. 7**. Variation of total sensitivity of each layer at different shear wave velocity ratios of the HVL placed at the 4th layer.

### 4.4 Discussion and Conclusion

Local search methods or Jacobian based inversion methods are most commonly used in surface wave inversion due to their computational speed. The detectability of any subsurface layer through inversion depends on how much a small perturbation of the layer properties affects the forward modeling. A layer with high sensitivity has a great chance of being easily identified. On the other hand, low sensitive layers don't significantly affect the dispersion energy, so there is a less chance of reconstruction. Irregular layers such as LVL and HVL are widely observed in near surface earth models. Rayleigh wave phase velocities are highly sensitive to the LVL.

This study analyzed the influence of stiff layers on the dispersion characteristics of vertical component Rayleigh wave. The sensitivity and dispersion spectrum are studied by placing the stiff layer at various depths and changing the velocity contrast. The sensitivity analysis of the HVL profiles shows that the HVL is poorly sensitive on the dispersion spectrum. The sensitivity effects get amplified with the increment of stiffness contrast of HVL with the neighboring layers. The stiff layers at shallow depth with high velocity contrast excide the higher modes at low frequency. Whereas, at high depth, the stiff layer doesn't much affect the energy of the dispersion spectrum. The low sensitivity causes an inverted shear wave velocity profile with low confidence. In this study only the vertical component of the Rayleigh wave is studied and observed that the vertical component is unable to capture the presence of a stiff layer at a deeper depth. Further study is needed to understand the stiff layer sensitivity on the transverse component of the Rayleigh wave and Love wave.

## References


1. Foti, S., Hollender, F., Garofalo, F., Albarello, D., Asten, M., Bard, P.-Y., Comina, C., Cornou, C., Cox, B., Di Giulio, G., Forbriger, T., Hayashi, K., Lunedei, E., Martin, A., Mercerat, D., Ohrnberger, M., Poggi, V., Renalier, F., Sicilia, D., Socco, V.: Guidelines for the good practice of surface wave analysis: a product of the InterPACIFIC project. Bulletin of Earthquake Engineering. 16, 2367–2420 (2018). https://doi.org/10.1007/s10518-017-0206-7.
2. Xia, J., Xu, Y., Luo, Y., Miller, R.D., Cakir, R., Zeng, C.: Advantages of Using Multichannel Analysis of Love Waves (MALW) to Estimate Near-Surface Shear-Wave Velocity. Surveys in Geophysics. 33, 841–860 (2012). https://doi.org/10.1007/s10712-012-9174-2.
3. Kumar, J., Naskar, T.: Effects of site stiffness and source to receiver distance on surface wave tests′ results. Soil Dynamics and Earthquake Engineering. 77, 71–82 (2015). https://doi.org/10.1016/j.soildyn.2015.04.022.
4. Mi, B., Xia, J., Shen, C., Wang, L.: Dispersion Energy Analysis of Rayleigh and Love Waves in the Presence of Low-Velocity Layers in Near-Surface Seismic Surveys. Surveys in Geophysics. (2018). https://doi.org/10.1007/s10712-017-9440-4.
5. Dal Moro, G.: The magnifying effect of a thin shallow stiff layer on Love waves as revealed by multi-component analysis of surface waves. Scientific Reports. 10, 9071 (2020). https://doi.org/10.1038/s41598-020-66070-1.

6. Xia, J., Miller, R.D., Park, C.B.: Estimation of near-surface shear-wave velocity by inversion of Rayleigh waves. Geophysics. 64, 691–700 (1999). https://doi.org/10.1190/1.1444578.
7. Pan, L., Chen, X., Wang, J., Yang, Z., Zhang, D.: Sensitivity analysis of dispersion curves of Rayleigh waves with fundamental and higher modes. Geophysical Journal International. 216, 1276–1303 (2019). https://doi.org/10.1093/gji/ggy479.
8. Ikeda, T., Matsuoka, T., Tsuji, T., Nakayama, T.: Characteristics of the horizontal component of Rayleigh waves in multimode analysis of surface waves. Geophysics. 80, EN1–EN11 (2015). https://doi.org/10.1190/GEO2014-0018.1.
9. Strobbia, C.: Surface Wave Methods - Acquisition, processing and inversion. (2003).
10. Naskar, T., Kumar, J.: Predominant modes for Rayleigh wave propagation using the dynamic stiffness matrix approach. Journal of Geophysics and Engineering. 14, 1032–1041 (2017). https://doi.org/10.1088/1742-2140/aa6fe3.
11. Shen, C., Xu, Y., Pan, Y., Wang, A., Gao, L.: Sensitivities of phase-velocity dispersion curves of surface waves due to high-velocity-layer and low-velocity-layer models. Journal of Applied Geophysics. 135, 367–374 (2016). https://doi.org/10.1016/j.jappgeo.2016.10.017.
12. Virieux, J.: P-SV wave propagation in heterogeneous media: Velocity-stress finite-difference method. GEOPHYSICS. 51, 889–901 (1986). https://doi.org/10.1190/1.1442147.
13. Moczo, P., Robertsson, J.O.A., Eisner, L.: The Finite-Difference Time-Domain Method for Modeling of Seismic Wave Propagation. Advances in Geophysics. 48, 421–516 (2007). https://doi.org/10.1016/S0065-2687(06)48008-0.
14. Park, C.B., Miller, R.D., Xia, J.: Multichannel analysis of surface waves. Geophysics. 64, 800–808 (1999). https://doi.org/10.1190/1.1444590.
15. Naskar, T., Kumar, J.: MATLAB codes for generating dispersion images for ground exploration using different MASW transforms. Geophysics. 1–37 (2022). https://doi.org/10.1190/geo2020-0928.1.
16. Mukherjee, S., Bhaumik, M., Naskar, T.: S-transform based processing of noisy surface wave record for recovering high-resolution spectrum. In: Second International Meeting for Applied Geoscience & Energy. pp. 2631–2635. Society of Exploration Geophysicists and American Association of Petroleum Geologists (2022). https://doi.org/10.1190/image2022-3751077.1.
17. Kausel, E., Roësset, J.M.: Stiffness matrices for layered soils. Bulletin of the Seismological Society of America. 71, 1743–1761 (1981). https://doi.org/10.1785/BSSA0710061743.
18. Kumar, J., Naskar, T.: A fast and accurate method to compute dispersion spectra for layered media using a modified Kausel-Roësset stiffness matrix approach. Soil Dynamics and Earthquake Engineering. 92, 176–182 (2017). https://doi.org/10.1016/j.soildyn.2016.09.042.
19. Naskar, T., Kumar, J.: A faster scheme to generate multimodal dispersion plots for Rayleigh wave propagation. Soil Dynamics and Earthquake Engineering. 117, 280–287 (2019). https://doi.org/10.1016/j.soildyn.2018.11.024.